Title

Detachment of compliant films adhered to stiff substrates via van der Waals interactions: role of frictional sliding during peeling

Journal

Journal of The Royal Society Interface, 11(97)

ISSN

1742-5689

Authors

Collino, Rachel R
Philips, Noah R
Rossol, Michael N
et al.

Publication Date

2014-08-06

DOI

10.1098/rsif.2014.0453

Peer reviewed

JOURNAL OF THE ROYAL SOCIETY Interface

rsif.royalsocietypublishing.org

Research

Cite this article: Collino RR, Philips NR, Rossol MN, McMeeking RM, Begley MR. 2014 Detachment of compliant films adhered to stiff substrates via van der Waals interactions: role of frictional sliding during peeling. *J. R. Soc. Interface* **11**: 20140453.
http://dx.doi.org/10.1098/rsif.2014.0453

Received: 30 April 2014
Accepted: 23 May 2014

Subject Areas:
bioengineering, biomaterials

Keywords:
peel test, thin-film adhesion, slip, friction, poly (dimethylsiloxane), digital image correlation

Author for correspondence:
Matthew R. Begley
e-mail: begley@engr.ucsb.edu

Electronic supplementary material is available at http://dx.doi.org/10.1098/risf.2014.0453 or via http://rsif.royalsocietypublishing.org.

Royal Society Publishing

Detachment of compliant films adhered to stiff substrates via van der Waals interactions: role of frictional sliding during peeling

Rachel R. Collino[1], Noah R. Philips[2], Michael N. Rossol[2], Robert M. McMeeking[1,2,3,4] and Matthew R. Begley[1,2]

[1]Department of Mechanical Engineering, and [2]Department of Materials, University of California, Santa Barbara, CA, USA
[3]School of Engineering, University of Aberdeen, King's College, Aberdeen AB24 3UE, UK
[4]INM—Leibniz Institute for New Materials, Campus D22, 66123 Saarbrücken, Germany

The remarkable ability of some plants and animals to cling strongly to substrates despite relatively weak interfacial bonds has important implications for the development of synthetic adhesives. Here, we examine the origins of large detachment forces using a thin elastomer tape adhered to a glass slide via van der Waals interactions, which serves as a model system for geckos, mussels and ivy. The forces required for peeling of the tape are shown to be a strong function of the angle of peeling, which is a consequence of frictional sliding at the edge of attachment that serves to dissipate energy that would otherwise drive detachment. Experiments and theory demonstrate that proper accounting for frictional sliding leads to an inferred work of adhesion of only approximately $0.5\,\mathrm{J\,m^{-2}}$ (defined for purely normal separations) for all load orientations. This starkly contrasts with the interface energies inferred using conventional interface fracture models that assume pure sticking behaviour, which are considerably larger and shown to depend not only on the mode-mixity, but also on the magnitude of the mode-I stress intensity factor. The implications for developing frameworks to predict detachment forces in the presence of interface sliding are briefly discussed.

1. Introduction

Many biological adhesive systems require surprisingly large forces to drive detachment, despite having relatively 'weak' interfaces with intrinsically low-energy interactions. Examples include the ability of geckos to adhere tenaciously to surfaces [1–6], the bio-fouling of polymers with bacteria [7,8] and the adhesion of mussels to rock [9]. In such systems, the energy associated with van der Waals interactions (e.g. geckos) or weak bonds (e.g. plants or mussels) is relatively low, yet one observes large forces required for detachment (i.e. peeling). Understanding the origins of large detachment forces in the presence of weak bonds has important implications for technological systems, such as the development of surgical glue or the adhesion of graphene to itself [10] and other substrates [11].

The force required to disconnect two surfaces depends not only on the interface bonding, but also on the presence of dissipative mechanisms at the interface and/or in the bulk of either material. Notable examples include plasticity or viscoelasticity either in the bulk or in thin interlayers joining the components; the presence of these mechanisms imply that the externally applied work required to detach part of the interface will be much larger than the work required to break bonds (on a per unit area basis). However, even in systems in which such dissipative mechanisms are absent, there can be a large discrepancy between the macroscopically inferred interface energy

and that associated with molecular-level debonding. In purely elastic systems without material dissipation, friction is an obvious source of dissipation that can dramatically alter detachment forces. Here, we demonstrate this to be the case in a 'dry' system (where no interfacial layer or adhesive exists between the film and substrate), in which the interface is bonded at the molecular level through relatively weak hydrogen or dipole-related bonding.

The above comments highlight the importance of distinguishing between adhesion energies that reference molecular-level debonding versus those that reference macroscopic behaviour, as the latter will be influenced by dissipation. Regardless of the choice, weak bonding does not mean 'weak adhesion' in the global sense. Here, we choose to define the adhesion energy (γ_i) as the energy per unit surface area required to separate a material interface at the molecular level through purely normal separation. For van der Waals interactions between an elastomer and glass, this adhesion energy has been measured via Johnson–Kendall–Roberts tests and pressurized blister (bulge) tests and is relatively low ($\gamma_i \sim 0.01 - 0.5\,\mathrm{Jm}^{-2}$) [12,13]. Nevertheless, pull-off forces in elastomer structures can be quite high [14,15], especially when forces tangential to the interface are applied [3]. This is true even for materials with little to no viscoelastic or plastic dissipative behaviour (such as poly(dimethylsiloxane) (PDMS), as studied here under low strain rates), strongly suggesting that frictional sliding at the interface is responsible.

The peel test is a common proxy for adhesion of geckos [1–6] or mussel plaques [9]. Similar peel geometries have been used to analyse gecko adhesion, for example, using adhesive tapes [3] and setal arrays of live geckos [4], and it has been postulated that both the geometry [3,4] and the motion of the foot [2] impact the animal's ability to cling. The classic peeling model set forth by Kendall [16,17] (and extended to large deformation by Molinari & Ravichandran [18] and Kim & Aravas [19]) assumes pure sticking at the interface and yields a very different angular dependence of the critical peel force if a single value for the work of separation is used. Alternatively, one may define a mixed-mode interface toughness that depends on the relative magnitudes of K_I (the stress intensity factor associated with normal stresses at the interface) and K_II (the stress intensity factor associated with shear stresses at the interface). As is well known from the thin-film literature, the relative magnitudes of K_I and K_II depend strongly on peel angle [20–22].

The importance of frictional sliding near the edge of a bonded interface has long been appreciated by the composites [23] and coating communities [24]. In such systems, which involve relatively stiff materials, frictional sliding occurs over very small distances compared with the feature dimensions; as such, the typical approach is to lump any contribution of frictional dissipation into the mixed-mode toughness. This approach becomes problematic when the frictional sliding zone size becomes comparable to a feature dimension (e.g. coating or lamina thickness), because it violates the presumption that the fracture process zone is controlled entirely by asymptotic fields and that toughness is independent of specimen geometry. While there have been insightful computational studies on the role of frictional sliding in altering crack-tip stress intensity factors [25,26], a consistent theory that quantifies mixed-mode toughness in terms of friction parameters is yet to emerge. This work is entirely consistent with previous studies of mixed-mode fracture, in the sense that it is recognized that friction will alter the conditions required to debond the interface. However, instead of implicitly lumping frictional dissipation into the toughness (as is commonly done for stiff composites and coatings), here, it is explicitly accounted for when computing the driving force. The net result is that debonding is predicted using a single interface toughness; a mixed-mode toughness is not needed, since the frictional contribution to debonding is accounted for in the driving force. As will be demonstrated, consistency between the experiments and Kendall-type models with mixed-mode interfacial toughness can only be achieved by invoking an interface toughness that depends strongly on film thickness and the inferred value of opening mode stress intensity factor K_I, even when $K_\mathrm{I} < 0$ (which implies contact occurs in the detached region just ahead of the edge of detachment).

It should be noted that the peel test has been used extensively to characterize adhesion in other systems [27–33], and for the case of dry elastomer/substrate interfaces in the adhesion of cling films [34,35]. Notably, examples which touch upon similar phenomena focus on tapes with additional adhesive layers or surface functionalization designed to promote attachment [3,33,36–40]. These works are highlighted in the extensive literature on peeling because of their focus on the role of interfacial slip during the peel process and its contribution to apparent work of adhesion. (Additional peeling references with an emphasis on delamination mechanics are given in [41].) In many of these studies, fluorescent beads are embedded in the tape or adhesive layer, and interfacial slip is observed by tracking individual beads dispersed in the film. In most cases, artificially 'mobile' viscoelastic or liquid-like layers grafted on the glass surface are used to induce observable slip displacements. In a similar vein, Blum *et al.* [40] studied the peeling of a commercial adhesive tape with an additional polymer film between the tape and the substrate, and observed lower peeling forces for polymer interlayers with higher segmental mobilities. Thus, experimental studies of interfacial sliding have been limited to peeling with viscous or viscoelastic layers, presumably enhancing the effect of slip; here, the focus is on the role of sliding in a dry elastic tape system.

2. Material and methods

2.1. Experimental and theoretical approach

In this work, we experimentally characterize peeling of a thin elastomer (PDMS) film from a glass substrate, with the goal of understanding the interplay between local adhesion energy (defined for purely normal separation), interface sliding, and the force to drive detachment. A schematic of these experiments is shown in figure 1. An elastomer film (or tape) is attached to the substrate only through van der Waals interactions; a clean dry film is pressed into contact with a clean, dry glass slide. One end of the tape is displaced at an angle θ between the detached portion and substrate, and the force F_c is measured. The applied displacement leads to peeling and stretching of the film in the direction parallel to θ and induces sliding in a portion of the film that is adhered to the substrate. Here, we present experimental evidence of small-scale slip in adhered films and its implication on the evolution of peel forces, within a framework that explicitly accounts for frictional sliding. We demonstrate that the force required for peeling can be accurately predicted as a function of peel angle using the local adhesion energy

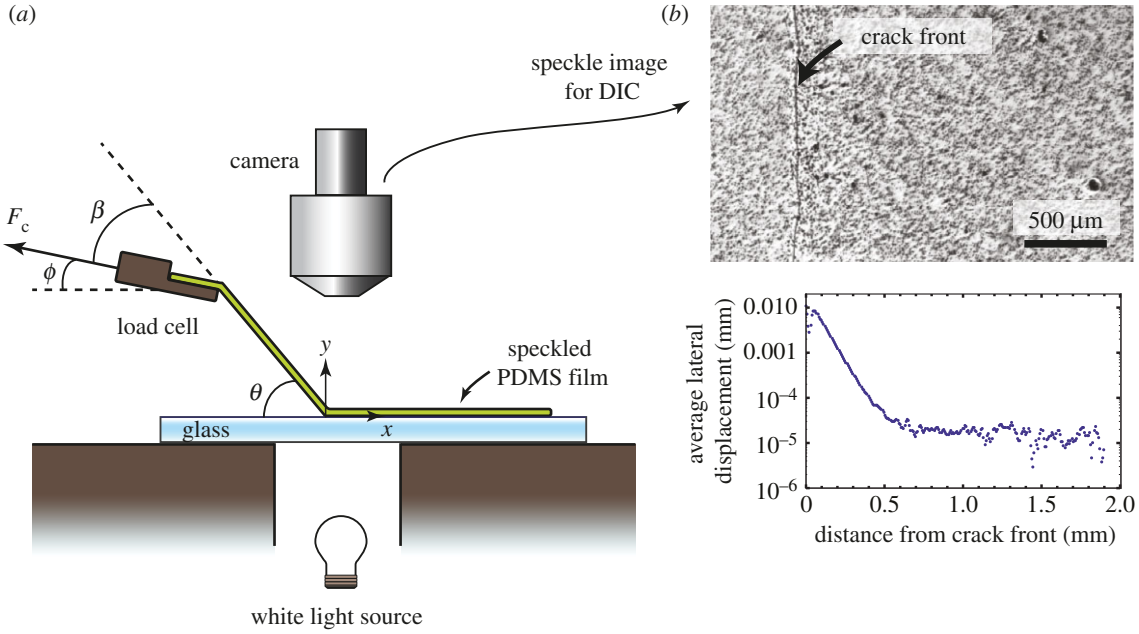

Figure 1. (*a*) Schematic of the peel test set-up. A speckled PDMS film is adhered to a glass slide with one end clamped to a load cell fixture. The load point is moved via a linear stage at a constant angle (ϕ); the film angle (θ) changes as the test progresses. (*b*) Displacements in the adhered region of the film near the crack front are measured via DIC. (Online version in colour.)

(γ_i, controlling purely normal separation), using a peeling model that accounts for frictional sliding in the adhered region.

2.2. Poly(dimethylsiloxane) films: fabrication and characterization

PDMS films were prepared by spin-coating precursor solutions from a commercial kit consisting of a base and curing agent (Dow Corning Sylgard 184) mixed with a 10 : 1 ratio, respectively. Prior to spin-coating, the mixed solutions were degassed in a vacuum desiccator for approximately 30 min. Thicknesses of approximately 50 and 80 µm were achieved by spin-coating the precursor on Si substrates for 1 min at 1125 and 750 r.p.m., respectively. A film thickness of approximately 125 µm was achieved by layering films spin-coated at 750 r.p.m. and 1500 r.p.m. Immediately prior to spin-coating, a few drops of a release agent (Jersey-Cote, LabScientific, Inc.) were applied to the Si substrate and spun at 3500 r.p.m. for 30 s. After spin-coating, the PDMS films were cured for 1 h at 80°C. Film thicknesses were measured by optical interferometry (Wyko NT1100, Veeco Instruments, Inc.).

As-cast films were transferred to glass substrates, cut to 25.4 mm strips, and speckled to allow for digital image correlation (DIC) [42]. A high-contrast speckle pattern was applied by brushing laser printer toner across the surface of PDMS films with a foam applicator. Speckles were fused to the PDMS film by placing the substrates onto a heated surface (120°C) for 75 s. After heating, the films were allowed to cool to room temperature and placed on borosilicate glass substrates previously cleaned with methanol. In all cases, the films were transferred by peeling gently from the parent substrate with tweezers, and laying on the test substrate slowly to avoid pre-strain as well as 'bubbles' (localized unbonded areas).

The tensile response of the as-cast, heated and speckled-plus-heated films was measured to illustrate the modest impact of the toner patterning on the mechanical properties of the PDMS films; details are provided in appendix A and data are provided in electronic supplementary material. The films are shown to exhibit neo-Hookean response with a shear modulus of $\mu \approx 0.5$ MPa (see table 2 in appendix A).

2.3. Peel tests

Peel testing was conducted at room temperature using the set-up illustrated in figure 1. The detached end of the PDMS film was clamped to a custom-made fixture attached to the load cell (Futek FSH00103). A screw-driven linear stage with a step size of 0.5 µm (T-LSR150B, Zaber Technologies) was used to pull the load cell fixture at a constant rate of 9 µm s^{-1} or less, and the load was recorded with a USB transceiver (Futek FSH03456). The stage's angle relative to the substrate, ϕ, is not necessarily equal to the peeling angle at any instant: the offset angle β is defined as: $\beta = \theta - \phi$; in the analysis that follows, we assume steady-state peeling, in which case $\beta \approx 0$. We also assume that the film is thin enough (and the detached length large enough) that the film may be treated as a membrane: for example, it is shown in [43] that bending effects can lead to discrepancies between the peel angle observed far from, versus immediately adjacent to, the peel front. For the following analysis, we assume that the film cannot support a bending moment (although the implications of small-scale bending are discussed in §4).

The location of the crack front is highlighted using the shadowgraph technique [44] which is sensitive to the second derivative (i.e. the Laplacian) of refractive index; strong contrast is generated by the discontinuity at the peel front, as shown in figure 1*b*. Plan-view images of the peel front- and side-view images of the peel angle were collected simultaneously using cameras with CCD resolution of 2048 × 2448 pixels (GRAS-50S5M-C, Point Grey Research). Displacements in the attached film were measured by applying DIC between plan-view images of the speckled PDMS film in undeformed and deformed states, using Vic-2D software.[1] At each angle measured, the displacement field is calculated by comparing the deformed image to the undeformed image in Vic-2D. Rigid body displacements (e.g. due to small movements of the camera or sample stage) were subtracted out of the extracted displacement field. The average displacement as a function of distance from the peel front in each image was analysed using an in-house-written *Mathematica*[2] code. Displacements were averaged along line scans, approximately 1 mm in

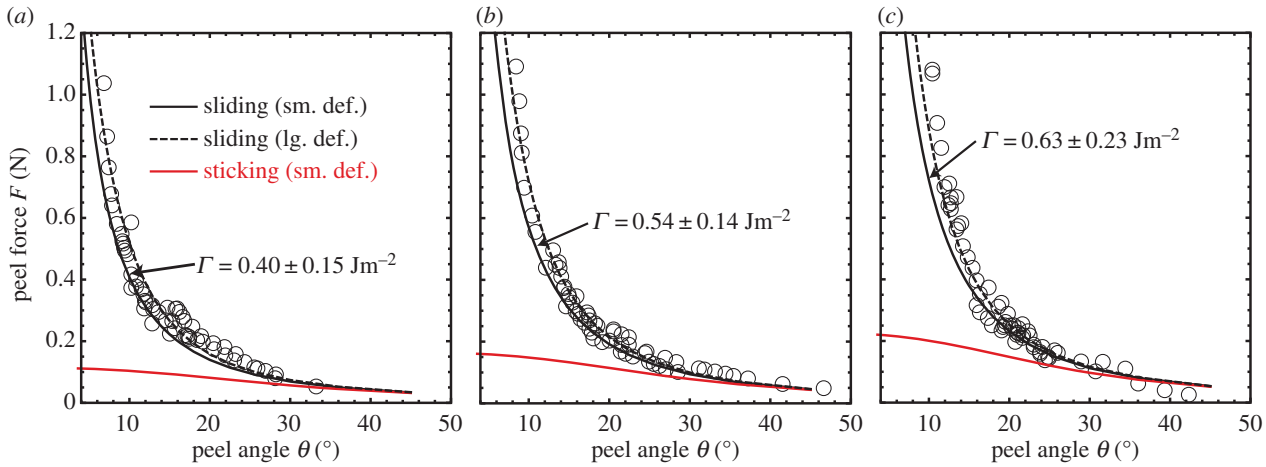

Figure 2. Peel force versus peel angle for (*a*) 50, (*b*) 80 and (*c*) 125 μm thick films. At angles approximately less than 30°, the data are in much better agreement with predictions for the critical peeling force from the present 'sliding' model (solid and dashed black lines for the small and large deformation models, respectively) as compared to Kendall's 'sticking' model coupled with a constant adhesion energy. In all cases, experimental error bars are smaller than the plotting points. The toughness values shown correspond to least-squares fits of the data to the small deformation sliding model, for each film thickness. (Online version in colour.)

width, taken parallel to the crack front and extending through the attached film.

3. Model

3.1. Peeling propagation for sliding and pure sticking

Recently, our group described a model for peeling assuming slip occurs in the adhered region. Tension applied to the end of the detached portion of the tape leads to peeling, stretching and sliding in the adhered tape near the edge of attachment. The model is for pure membrane behaviour (i.e. it neglects bending, as in the Kendall model), allows for large deformation, and it is assumed that the peel angle θ matches the angle of the applied force. (In the discussion that follows, we validate that membrane solutions are applicable for the dimensions tested here.) Steady-state peeling is assumed when the energy released by peeling is equal to the work of separation for *purely normal* displacements. As such, in this analysis, any work done by friction is balanced by a corresponding increase in the work done by the applied load and the shear sliding stress does not appear explicitly in the following equations. The energy release rate G of a peeling film undergoing frictional sliding, and assuming large deformations, is given by [41]

$$G_s = \frac{F}{w}(\lambda_D - \lambda_A \cos\theta) + h(\psi(\lambda_A) - \psi(\lambda_D)), \tag{3.1}$$

where F is the applied force, w and h are the undeformed film width and thickness, respectively, λ_D is the stretch of the film in the detached region and λ_A is the axial stretch ratio of the attached portion of the film at the edge of the attached region ($x = 0$ in figure 1). The function ψ describes the strain energy density in the film as a function of stretch; for a neo-Hookean material [45] subjected to plane strain conditions, one obtains

$$\psi(\lambda) = \frac{\mu}{2}\left(\lambda^2 + \frac{1}{\lambda^2} - 2\right), \tag{3.2}$$

where, in general, λ is the axial stretch ratio. This function can be used to derive the force in the tape in terms of the stretch ratio, using $F = wh(\partial\psi/\partial\lambda)$. The two stretch ratios, λ_A and λ_D, are then given by the solutions to

$$F = wh\mu\left(\lambda_D - \frac{1}{\lambda_D^3}\right) \quad \text{and} \quad F\cos\theta = wh\mu\left(\lambda_A - \frac{1}{\lambda_A^3}\right). \tag{3.3}$$

Equations (3.1) and (3.2) allow one to determine the critical force for peeling as a function of peel angle, by solving for F such that $G_s = \gamma_i$; equations (3.3) must be solved numerically to obtain the stretch ratios corresponding to a given force. The results presented in figures 2 and 3 labelled 'large deformation' were generated using this procedure and the root-finding algorithms in *Mathematica* (see endnote 2).

The above predictions for sliding are to be contrasted with those assuming pure sticking. In [41], we present the corresponding large deformation result for pure sticking (i.e. Kendall's model but accounting for large deformation)

$$G_K = \frac{F}{w}(\lambda_D - \cos\theta) - h\psi(\lambda_D), \tag{3.4}$$

which can be obtained from the general result by noting that sticking implies $\lambda_A = 1$ and $\psi(1) = 0$.

Both the sliding model (equation (3.1)) and the sticking (Kendall) model (equation (3.4)) can be simplified considerably for small deformations. Making the substitution $\lambda = 1 + \varepsilon$, where ε is the strain in the film, and expanding the result for $\varepsilon \ll 1$, we find that the above sliding equations reduce to [41]

$$\bar{F}_s = \frac{1}{\sin\theta}\left(\sqrt{2\bar{\Gamma}_i + \tan^2\frac{\theta}{2}} - \tan\frac{\theta}{2}\right), \tag{3.5}$$

where $\bar{F}_s = F_s/(Ewh)$ with $E = 3\mu$ being Young's modulus of the film, and $\bar{\Gamma}_i = \gamma_i/(Eh)$. The analogous small deformation result for the pure sticking model is obtained by normalizing Kendall's classic result in [17], where $\bar{F}_K = F_K/(Ewh)$

$$\bar{F}_K = \sqrt{2\bar{\Gamma} + 4\sin^4\frac{\theta}{2}} - 2\sin^2\frac{\theta}{2} \tag{3.6}$$

The small deformation results highlight a critical difference between sliding and sticking assumptions; in the limit of $\theta \to 0$, and for a constant interface energy required for debonding,

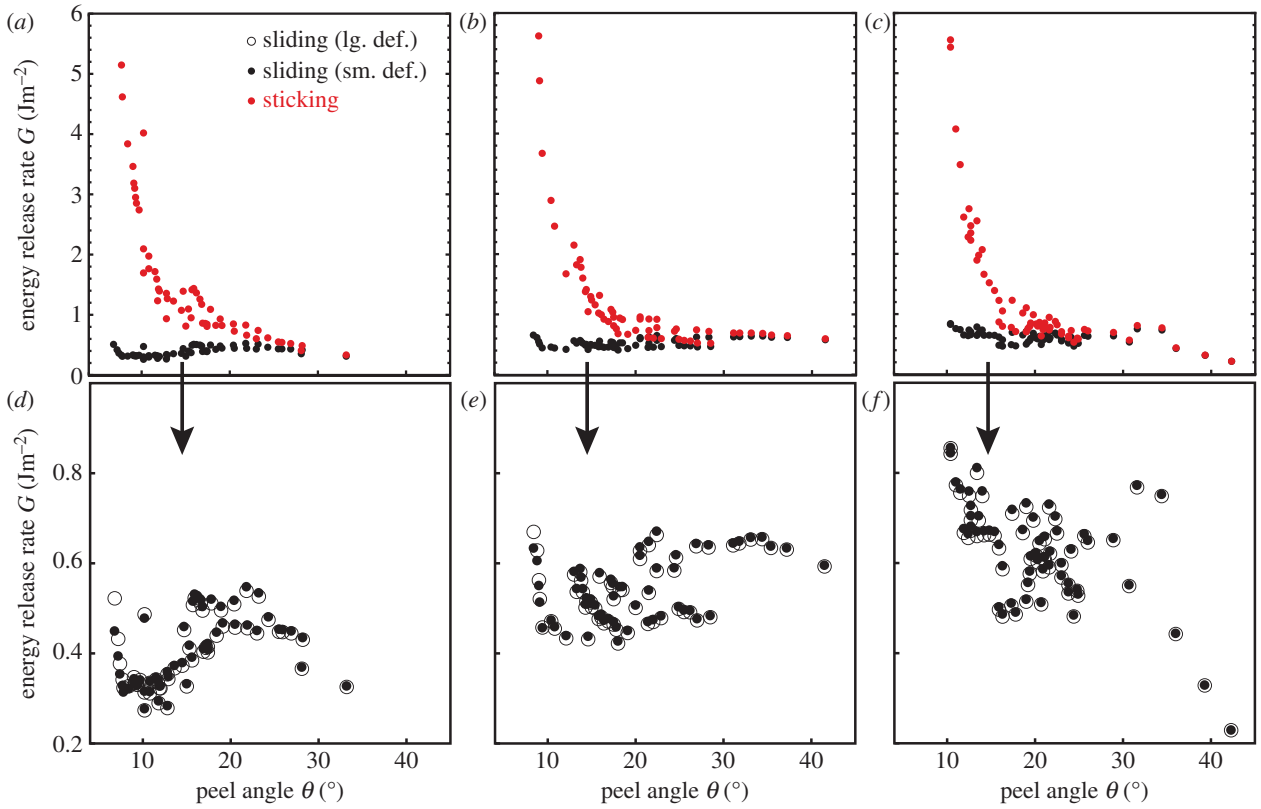

Figure 3. Energy release rate versus peel angle predicted from sticking and sliding models of peeling for (*a*,*d*) 50, (*b*,*e*) 80 and (*c*,*f*) 125 µm thick films. In (*a*–*c*), the energy release rate values predicted by sticking and sliding models diverge at intermediate angles (approx. 20°). (*d*–*f*) On a smaller scale, the energy release rates predicted from large deformation (open symbols) and small deformation (filled symbols) sliding models, highlighting the similarity in calculated values at all but the smallest peel angles. (Online version in colour.)

the critical force for peeling with pure sticking asymptotes to a finite value $\left(F_K \to w\sqrt{2\gamma_i Eh}\right)$. For the case in which the film slides near the delamination front, $F_s \to \infty$ as $\theta \to 0$. In the sliding approach, peeling is dictated only by the force normal to the substrate, and as a result, larger peel forces are predicted as the angle decreases.

3.2. Displacement distributions in the sticking portion of the film

To aid in interpreting the DIC measurements, we present an approximate model for the displacement of the surface of the film in the *sticking* region in the adhered portion of the film; discrepancies between the measured displacements and the displacements arising from this sticking model yield insight regarding the length-scale over which sliding occurs. For the sticking model, we assume that the displacements in the film in the adhered region are given by

$$u(x, y) = \frac{2u_s(x)}{h}\left(y - \frac{y^2}{2h}\right), \tag{3.7}$$

where x is measured from the edge of the sticking region, $u_s(x)$ is the displacement at the top surface of the film and y is the distance from the interface to a point in the film, as shown schematically in figure 1. Note that $u(x, 0) = 0$ is the displacement along the interface, as implied by sticking. This produces a shear strain distribution in the film given by

$$\gamma(x, y) = \frac{2u_s(x)}{h}\left(1 - \frac{y}{h}\right). \tag{3.8}$$

The shear strain is zero at the top surface of the film (because there is no shear stress acting there), and the shear strain at the interface is $\gamma_i = 2u_s(x)/h$. The factor of two arises because it is assumed that the shear strain varies linearly from the interface to the surface; the *average* shear strain in the film is $\langle\gamma(x)\rangle = u_s(x)/h$. The strain energy in the system, for plane strain conditions and small deformations, is given by

$$\Pi = \int_0^L \left[\int_0^h \left(\frac{E\varepsilon^2}{2(1-\nu^2)} + \frac{E\gamma^2}{4(1+\nu)}\right) \mathrm{d}y\right] \mathrm{d}x. \tag{3.9}$$

For Poisson's ratio $\nu = 1/2$ and the displacements assumed above, taking the first variation with displacement boundary conditions imposed at $x = 0$ and $x = L$ yields

$$\frac{\mathrm{d}^2 u_s}{\mathrm{d}x^2} - \frac{5}{8}\frac{u_s}{h^2} = 0. \tag{3.10}$$

The solution to the governing equation is then

$$u_s(\bar{x}) = A\mathrm{e}^{-\bar{x}}, \tag{3.11}$$

where $\bar{x} = x/x_o$ with $x_o = \left(\sqrt{8/5}\right)h$, and A is a constant determined from the boundary conditions at $x = 0$, the edge of the sticking portion of the interface. The key point is that the surface displacements in regions with a non-sliding interface can be expected to decay exponentially, with a decay length that is dictated solely by the thickness of the film. Deviations from this result near the edge of attachment may be attributed to sliding and bending of the film, as will be discussed in detail.

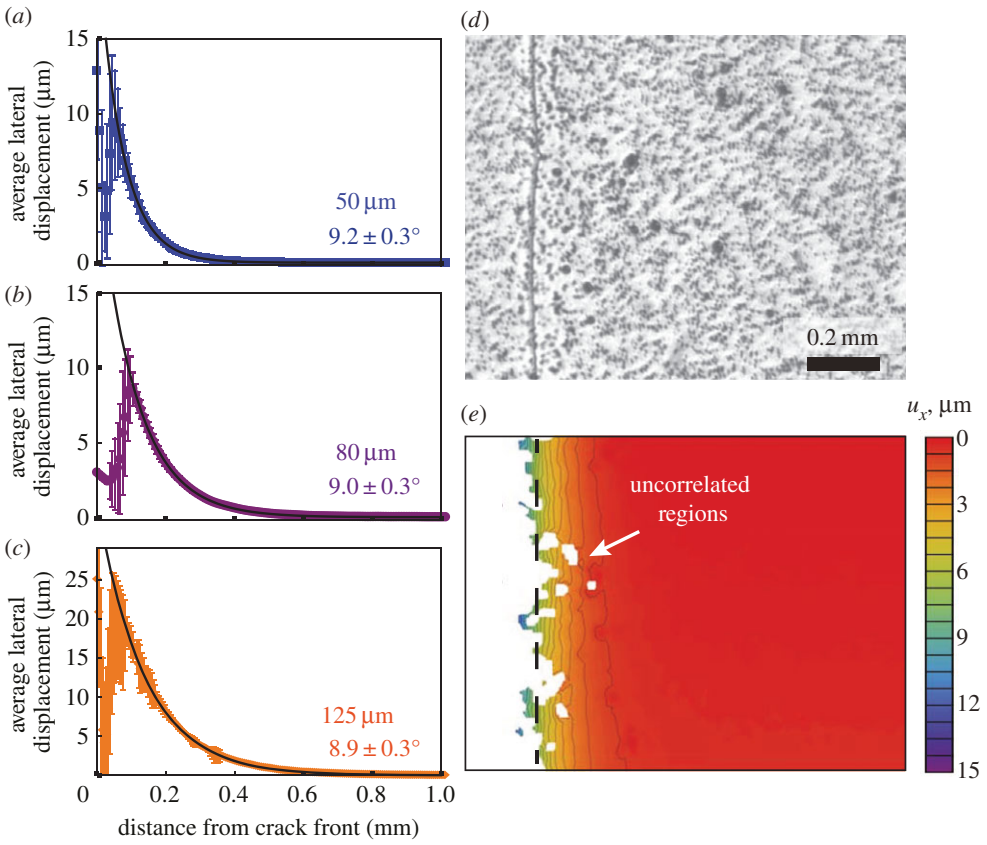

Figure 4. Lateral surface displacements determined via DIC for (*a*) 50, (*b*) 80 and (*c*) 125 μm thick films, measured at peel angles of approximately 9°. The solid line represents a least-squares fit of the data to an exponential decay function. For similar peel angles, characteristic decay length increases with increasing film thickness. (*d*) Image of a representative region near the crack front used to determine the displacement profile for the 50 μm thick film data in (*a*). (*e*) Contour plot of lateral displacement corresponding to the image in (*d*). The dashed line shows the approximate position of the crack front. White regions represent areas in which image correlation failed, leading to measurement uncertainty in the displacement near the edge of delamination.

4. Results and discussion

4.1. Peel tests and comparison of sliding and sticking models

The peel force as a function of the peeling angle is shown in figure 2 for (*a*) 50 (*b*) 80 and (*c*) 125 μm thick films. For each film thickness, the data were collected from samples cut from the same spin-coated film, and comprise at least four separate tests. The data are fit to the sliding model assuming large deformations (equations (3.1)– (3.3)) as well as the sliding (equation (3.5)) and sticking (equation (3.6)) models assuming small deformations; the fits are shown in figure 2 as black dashed lines, black solid lines and red solid lines, respectively. Interfacial toughness values of 0.40 ± 0.15 (0.40 ± 0.15), 0.54 ± 0.14 (0.54 ± 0.14) and 0.63 ± 0.23 (0.62 ± 0.22) Jm^{-2} are estimated from least-squares fits to the expression for the energy release rate determined from the small (large) deformation model for 50, 80 and 125 μm films, respectively, and represent the average and 2 s.d. from the mean.

For all film thicknesses, the predicted peel force for sliding and sticking models begins to diverge at intermediate peel angles (20°), with better agreement to sliding models at smaller peel angles. The interfacial toughnesses estimated here are slightly higher than those reported for plain PDMS on glass surfaces [12,13], possibly due to modification of the composition of the PDMS film surface from the application of speckles, which also results in an increase of the elastic modulus (see appendix A). The scatter in the data probably arises partly from the fact that the peel angle evolves slightly throughout the test, indicating that a portion of each test (which spans multiple peel angles) is not strictly at steady state. This is a consequence of the fact that the tests are conducted in displacement control. It is reasonable to expect that intermittent stick–slip behaviour also influences the scatter, although it must occur at length scales that are not readily observable.

Figure 3 presents estimates of the energy release rate as a function of peel angle for the small deformation sticking model as well as the small and large deformation sliding models for 50, 80 and 125 μm thick films, calculated for each data point from equations (3.4) and (3.1). The energy release rate predicted by fits of the data to the sliding model is relatively insensitive to peel angle when compared with the predictions from the sticking model, validating the sliding model approach for this case. In particular, figure 3*d–f* illustrates the similarity in the values calculated between the small and large deformation models at all but the smallest peel angles. One possible source for the scatter seen in figure 3*d–f* for the sliding models may be stick–slip behaviour in the debonding process zone, though the sliding zone is too small to resolve via surface displacements, as described next.

Lateral surface displacements measured via DIC in the attached region of the film are shown in figure 4*a–c* for 50, 80 and 125 μm thick films, respectively. The average lateral displacement is computed from displacements measured

across a line parallel to the crack front; error bars represent the standard deviation of the mean at each lateral distance. Image analysis was performed in the centre of the film; rounded crack fronts (due to edge effects) were observed at the outer boundaries of the film, but comprised less than 10% of the total film width. The lateral distance is measured from the optical contrast line created by the edge of attachment, seen clearly in figure 4*d*. In this case, the peel front is moving to the right: the area to the right of the contrast line is the region of the film attached to the substrate. This contrast line is also associated with the loss of correlation in the DIC fitting process, represented by the blank regions in figure 4*e*; note that in addition to the region in the wake of the crack (where the film is unattached and large out-of-plane displacements occur), there are also small localized regions ahead of the crack, in the attached portion of the film, where DIC correlation fails.

The relatively large uncertainties in measured displacement near the crack front in figure 4*a–c* result from this incomplete image correlation near the discontinuity, probably due to out-of-plane motion in the unattached portions of the film, as well as any bending that occurs in the attached portion of the film near the edge of delamination. The solid lines in figure 4*a–c* represent fits of the displacement to an exponential of the form given in equation (3.11), using the least-squares method, where $u_s(x)$ is the lateral displacement as a function of distance from the crack front measured via DIC, x_o is the characteristic decay length of the displacement, and A is a fitting constant. In each case, data associated with the noise inherent to the DIC process and data in areas in which DIC correlation failed (as discussed in §2) were truncated. Therefore, the data used in the fit included only those points between a distance of two film thicknesses away from the peel front, and the far edge of the noise floor (determined by average DIC displacements in stationary portions of the film, measured a few millimetres away from the peel front).

This characteristic decay length appears approximately constant for a given film thickness across the range of peel angles shown in figure 5 for 50, 80 and 125 µm thick films and appears to scale with film thickness. In each case, x_o is determined from exponential fits described above, with error determined from a weighted sum of squares, using standard deviation from the mean of lateral displacements measured via DIC. The data are in good agreement with the predicted characteristic decay distance for a fully-sticking film predicted by equation (3.11). This predicted decay distance, $x_o = 1.26h$, is shown by dashed lines in figure 5, suggesting that the majority of the film is sticking in the portion of the film modelled here ($x > 2$ h, as defined in figure 1). This theoretical decay distance slightly underestimates the data for the thinner films; this may be due to intermittent sliding.

Together with measurements illustrating the divergence of the peel force with decreasing peel angles and the agreement of peel force with sliding model predictions, the DIC results suggest that small-scale sliding occurs in the adhered portion of the film adjacent to the peel front. DIC measurements of the lateral surface displacements suggest that at distances larger than approximately two film thicknesses away from the crack front, the majority of the film is sticking (although intermittent large-scale sliding may occur). It is likely that most sliding occurs closer to the edge of delamination, within a distance of one or two film thicknesses, in a regime not well-captured by two-dimensional DIC. The details may be further complicated by bending effects not captured by the tape model employed here. One avenue for future work may be more detailed measurements via three-dimensional DIC, capturing through-thickness displacements closer to the interface.

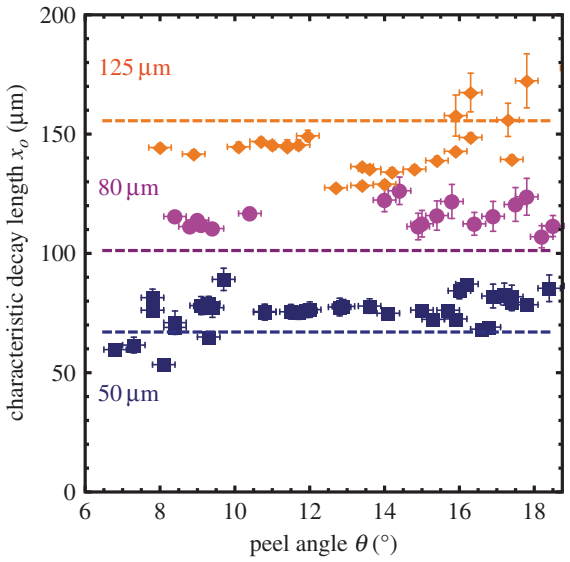

Figure 5. Measured displacements in the adhered region of the film near the crack front as a function of peel angle and film thickness. The dashed lines correspond to the predicted decay distance for a fully-sticking film, for each film thickness.

4.2. Mixed-mode fracture analysis of the peel test

It is interesting to illustrate the implications of the above experiments in the context of a mixed-mode interface fracture framework [20]. As elucidated by Hutchinson & Suo [46], the mode-I and mode-II stress intensity factors for a thin film debonding from an effectively infinite, rigid substrate may be given by

$$\left.\begin{aligned} K_{\mathrm{I}} &= -\frac{P}{\sqrt{2h}}\cos\omega + \frac{\sqrt{6}M_o}{h^{3/2}}\sin\omega \\ \text{and} \qquad K_{\mathrm{II}} &= -\frac{P}{\sqrt{2h}}\sin\omega - \frac{\sqrt{6}M_o}{h^{3/2}}\cos\omega, \end{aligned}\right\} \tag{4.1}$$

where P is the axial force resultant, M_o is the moment resultant acting at the crack tip and ω is a so-called phase factor that depends on elastic mismatch α. (For this case, with $\alpha = -1$, $\omega = \pi/4$. Note that the sign in front of P in the above is the opposite of that used in the definition of Hutchinson & Suo [46], since the peel force acts in the direction opposite to their definition of a positive axial force resultant.)

The moment acting at the crack tip for the peel test can be determined as a function of peel force in the limit that the length of the detached segment of tape is semi-infinite [22,47]. To verify that this limit is appropriate for an experiment with a finite length of detached film, one can solve for the deflection of a finite detached length of film using moderate rotation plate theory, which is valid for peel angles less than 30° [48]. The relevant results are

$$M_o = \sqrt{EIP}\,\theta \tanh\left[\sqrt{\frac{12PL^2}{Ebh^3}}\right] \tag{4.2}$$

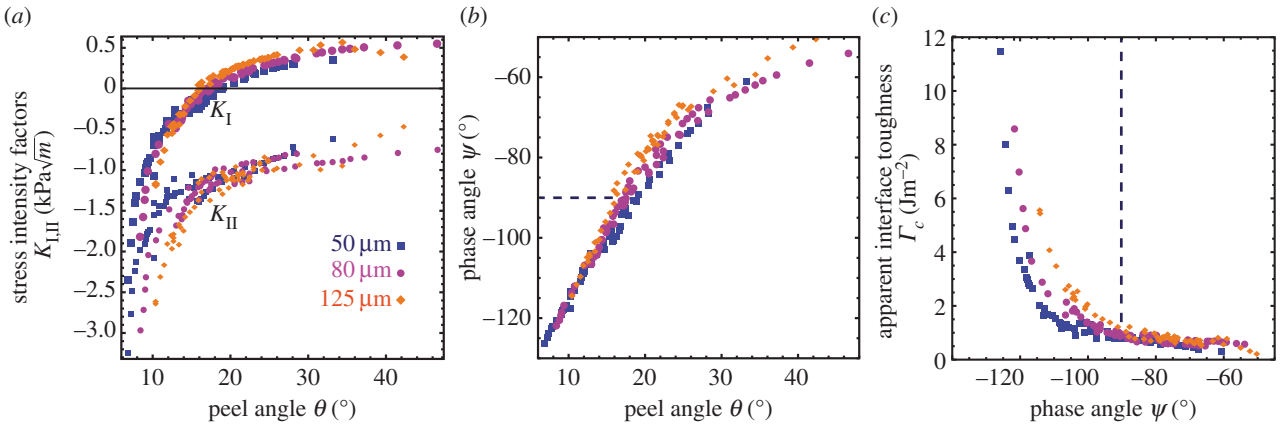

Figure 6. Mixed-mode fracture analysis of peeling. (*a*) Mode-I and mode-II stress intensity factors calculated from equations (4.1) with experimental peel forces, as a function of peel angle. (*b*) Phase angle as a function of peel angle and (*c*) apparent interface toughness as a function of phase angle. The symbols represent values calculated in a domain allowing $-180^\circ < \psi < -90^\circ$, whereas the dashed lines correspond to the convention of defining $\psi = -90^\circ$ when $K_I < 0$.

and

$$G = \frac{P^2}{2Ehb^2} + \frac{1}{2}\frac{P}{b}\theta^2 \tanh^2\left[\sqrt{\frac{12PL^2}{Ebh^3}}\right], \tag{4.3}$$

where b is the width of the tape, L is the length of the detached portion of the tape and $I = bh^3/12$. Noting that the $\lim_{\beta\to\infty} \tanh \beta = 1$ and that $\sin\theta_a \approx \theta_a$ (as required for moderate rotation theory), we can see that these results are identical to previous ones [22,47] for the crack-tip moment and the Kendall energy release rate, in the limit of an infinitely long film. The peel forces and dimensions in this experiment (where $L \approx 10$ mm) indicate that the tanh term is indeed effectively unity for the cases considered here. Hence, for all intents and purposes, the detached films in these experiments are effectively semi-infinite and membrane theory is applicable.

Using these definitions, we can compute the mode-I and mode-II stress intensity factors in the peel test, as shown in figure 6*a*: here, the experimentally measured values of peel force are used with equations (4.1). Note that K_I becomes negative for peel angles less than $\theta \approx 20^\circ$. (This is consistent with a theoretical case study by Thouless & Yang [21].) The corresponding phase angles are shown in figure 6*b* as a function of peel angle. Here, two definitions of phase angle are adopted: in the first (indicated with a dashed line), regions with $K_I < 0$ are defined to have $\psi = -90^\circ$ as has been suggested elsewhere [20,21], motivated by the fact that the crack will be closed in the region dominated by the elastic singularity. In the second, the inverse tangent function is defined to account for the quadrant in which K_I and K_{II} fall, such that $K_I < 0$ and $K_{II} < 0$ correspond to $-180^\circ < \psi < -90^\circ$. Figure 6*c* plots the interface toughness inferred via the Kendall result as a function of phase angle, i.e. the mixed-mode interface toughness relationship, for both of these phase angle definitions.

The results clearly demonstrate that regions with $K_I < 0$ correspond to large values of interface toughness, as inferred from the Kendall approach that assumes that all work dissipated in the debonding process zone can be lumped into the interface toughness. Of course, $K_I < 0$ implies that the region immediately adjacent to the crack tip is closed; when frictional sliding dominates dissipative mechanisms, it seems obvious that more negative K_I values will imply greater macroscopic toughness, since a larger region ahead of the nominal crack tip experiences sliding and therefore the amount of dissipated energy increases. It is clear from figure 6*c* that simply truncating the phase angle at $\psi = -90^\circ$ for all cases with $K_I < 0$ is problematic, as one would obtain a multi-valued interface toughness for scenarios defined as 'pure mode-II'.

While one might be tempted to simply extend the range of permissible phase angles to include regions with negative K_I, doing so likely undermines the presumption that the mixed-mode interface toughness is independent of specimen geometry. The size of the frictional sliding zone (and hence energy dissipated) will depend not only on K_I, but also on the nature of the transition from asymptotic displacements to the far field displacements (e.g. the detached film displacements), which will generally be dependent on specimen geometry. (Consider a bilateral strip loaded with normal and tangential far field displacements, as described by Liechti & Chai [49]. For this geometry, $K_I < 0$ likely implies far greater sliding zones, including the possibility that the entire interface is closed.)

Thus, it is unlikely that the toughness-phase angle relationship, regardless of how it is defined, is generally applicable to other geometries with frictional sliding, although it may be practically useful for geometries that are similar. It is worth noting that even for interfaces where plastic deformation dominates, the universality of a mixed-mode toughness has yet to be fully validated with multiple specimen types (as has been done for conventional fracture). This is no doubt a result of the fact that preparing different specimens with identical materials and interfaces, *and* conducting mixed-mode fracture tests over a broad range of phase angles, is an extremely daunting experimental challenge.

5. Concluding remarks

In this work, we present evidence of frictional sliding in elastomer films during the peeling process. These results suggest that frictional sliding may be an important dissipative mechanism in biological and technological systems in which strong adhesion is observed in otherwise 'weakly bonded' systems. Using DIC, we are able to observe surface displacements during the peel process which suggest that sliding is likely confined to a region within two film thicknesses of the peel front. Despite the apparently narrow sliding 'window', measurements of forces required for peeling across a broad range of

angles validate a model for the peeling process in which frictional sliding is explicitly accounted for when computing the energy release rate, as opposed to the classical 'pure sticking' models by Kendall.

Using a mixed-mode fracture framework, we illustrate that the presence of frictional sliding over length scales comparable to the film thickness raises questions about the efficacy of using a mixed-mode fracture toughness. The toughness is shown to be dependent on the magnitude of K_I, as opposed to simply the energy release rate and phase angle. This indicates that the present peeling process is analogous to large-scale yielding, in that the fracture (detachment) process is not controlled by asymptotic crack-tip fields. The concept of a mixed-mode fracture toughness approach is predicated on the assumption that K_I and K_{II} are sufficient to characterize the behaviour in the fracture process zone. Indeed, the asymptotic fields described by K_I and K_{II} will control the behaviour of the fracture process zone when it is small in comparison to feature dimensions (coating or lamina thickness). However, when sliding occurs over large length scales, the fracture process zone is influenced by behaviours outside the regions of K_I and K_{II} dominance, and the toughness becomes specimen-dependent. This is the case in these experiments; one does not obtain a constant toughness for cases with negative K_I, which is commonly defined as having a constant phase angle (-90°). While the sliding zone in these experiments is small in comparison to the detached tape length, it is comparable to the tape thickness; this implies that sliding behaviours will significantly influence the deformation over length scales much larger than those controlled by the asymptotic fields defined by K_I and K_{II}.

Funding statement. The authors gratefully acknowledge support from the National Science Foundation through award number CMMI-1063714. M.N.R. was supported in part by The Pratt and Whitney Center of Excellence at the University of California, Santa Barbara.

Endnotes

[1]Vic 2D Software 2007 Correlated Solutions Inc., Columbia, SC.
[2]Mathematica Version 8.0.4. 2011, Wolfram Research Inc., Champaign, IL

Appendix A. Modulus measurements of speckled poly(dimethylsiloxane)

As the elastic properties of PDMS films can vary widely depending on composition, curing schedule and precursor mixing ratios, the moduli of the films used here were measured directly. DIC allows for the measurement of shear modulus of speckled films but not unpatterned plain PDMS films. However, the effect of the speckles (either the heating process or the toner itself) on the film is unknown. To validate the DIC method and determine what effect the speckles have on the PDMS film modulus, blister tests [13] were conducted on as-cast, heated and speckled-plus-heated films to independently measure Young's modulus (E). Modified films were then tensile tested in the DIC set-up. Speckled films were cut into narrow strips (aspect ratio > 5) and pulled in the peel tester described above at a strain rate of less than 10^{-3} with peel angle of zero degrees (i.e. no peeling) while imaging for DIC and the subsequent computation of strains.

We find that for the speckled PDMS films, a neo-Hookean constitutive law captures the behaviour for the regimes studied here, as shown in figure 7 for uniaxial tension. The uniaxial response of such a material is

$$t_1 = \mu\left(\lambda_1 - \frac{1}{\lambda_1^2}\right), \tag{A 1}$$

where the nominal stress in the film, t_1, (measured directly as force divided by original cross-sectional area) is a function of the shear modulus μ and the axial stretch ratio, λ_1 (computed with DIC). With the assumption of incompressibility (implicit in equation (A 1)), the measured moduli are in good agreement with solutions to the blister test [13], as shown in table 1. Thus, the addition of the speckles causes an increase in the modulus that is not attributable to annealing during the fusion of the toner to the PDMS film. To account for the effect of the speckles (and that of any variations in speckle density), the modulus of each film was measured and input into the peeling calculations (table 2).

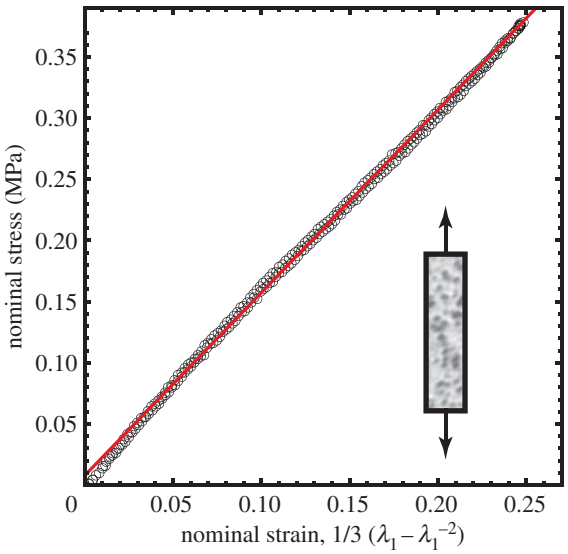

Figure 7. The uniaxial response of a speckled PDMS film is well characterized by a neo-Hookean constitutive law. (Online version in colour.)

Table 1. Effect of speckle application on modulus. Young's modulus E for a 157 μm thick PDMS in as-cast, heated and speckled-plus-heated states, as measured by DIC and validated by blister tests.

	$E_{blister}$ (MPa)	E_{DIC} (MPa)[a]
as-cast	0.98	n/a
heated	0.99	n/a
speckled-plus-heated	1.46	1.50

[a]Young's modulus calculated assuming incompressibility by measuring the shear modulus, μ, with DIC.

Table 2. Film properties. (Shear modulus μ for the films used in the peel tests, as measured by DIC.)

film thickness (μm)	μ (MPa)
53	0.464
80	0.468
123	0.498

References

1. Autumn K *et al*. 2002 Evidence for van der Waals adhesion in gecko setae. *Proc. Natl Acad. Sci. USA* **99**, 12 252–12 256. (doi:10.1073pnas.192252799)
2. Tian Y, Pesika N, Zeng H, Rosenberg K, Zhao B, McGuiggan P, Autumn K, Israelachvili J. 2006 Adhesion and friction in gecko toe attachment and detachment. *Proc. Natl Acad. Sci. USA* **103**, 19 320–19 325. (doi:10.1073/pnas.0608841103)
3. Pesika NS, Tian Y, Zhao B, Rosenberg K, Zeng H, McGuiggan P, Autumn K, Israelachvili JN. 2007 Peel-zone model of tape peeling based on the gecko adhesive system. *J. Adhesion* **83**, 383–401. (doi:10.1080/00218460701282539)
4. Gravish N, Wilkinson M, Autumn K. 2008 Frictional and elastic energy in gecko adhesive detachment. *J. R. Soc. Interface* **5**, 339–348. (doi:10.1098/rsif.2007.1077)
5. Chen B, Wu P, Gao H. 2009 Pre-tension generates strongly reversible adhesion of a spatula pad on substrate. *J. R. Soc. Interface* **6**, 529–537. (doi:10.1098/rsif.2008.0322)
6. Cheng QH, Chen B, Gao HJ, Zhang YW. 2012 Sliding-induced non-uniform pretension governs robust and reversible adhesion: a revisit of adhesion mechanisms of geckos. *J. R. Soc. Interface* **9**, 283–291. (doi:10.1098/rsif.2011.0254)
7. Razatos A, Ong Y-L, Sharma MM, Georgiou G. 1998 Molecular determinants of bacterial adhesion monitored by atomic force microscopy. *Proc. Natl Acad. Sci. USA* **95**, 11 059–11 064. (doi:10.1073/pnas.95.19.11059)
8. Ong Y, Razatos A, Georgiou G, Sharma M. 1999 Adhesion forces between *E. coli* bacteria and biomaterial surfaces. *Langmuir* **15**, 2719–2725. (doi:10.1021/la981104e)
9. Waite JH, Andersen NH, Jewhurst S, Sun C. 2005 Mussel adhesion: finding the tricks worth mimicking. *J. Adhesion* **81**, 297–317. (doi:10.1080/00218460590944602)
10. Lu Z, Dunn ML. 2010 van der Waals adhesion of graphene membranes. *J. Appl. Phys.* **107**, 044301. (doi:10.1063/1.3270425)
11. Koenig SP, Boddeti NG, Dunn ML, Bunch JS. 2011 Ultrastrong adhesion of graphene membranes. *Nat. Nanotechnol.* **6**, 543–546. (doi:10.1038/NNANO.2011.123)
12. Savkoor AR, Briggs GAD. 1977 Effect of tangential force on contact of elastic solids in adhesion. *Proc. R. Soc. Lond. A* **356**, 103–114. (doi:10.1098/rspa.1977.0123)
13. Sofla A, Seker E, Landers JP, Begley MR. 2010 PDMS–glass interface adhesion energy determined via comprehensive solutions for thin film bulge/blister tests. *J. Appl. Mech.* **77**, 031007. (doi:10.1115/1.4000428)
14. Spuskanyuk AV, McMeeking RM, Deshpande VS, Arzt E. 2008 The effect of shape on the adhesion of fibrillar surfaces. *Acta Biomater.* **4**, 1669–1676. (doi:10.1016/j.actbio.2008.05.026)
15. Paretkar D, Kamperman M, Martina D, Zhao J, Creton C, Lindner A, Jagota A, McMeeking R, Arzt E. 2013 Preload-responsive adhesion: effects of aspect ratio, tip shape and alignment. *J. R. Soc. Interface* **10**, 20130171. (doi:10.1098/?rsif.2013.0171)
16. Kendall K. 1971 Adhesion and surface energy of elastic solids. *J. Phys. D Appl. Phys.* **4**, 1186–1195. (doi:10.1088/0022-3727/4/8/320)
17. Kendall K. 1975 Thin-film peeling—elastic term. *J. Phys. D Appl. Phys.* **8**, 1449–1452. (doi:10.1088/0022-3727/8/13/005)
18. Molinari A, Ravichandran G. 2008 Peeling of elastic tapes: effects of large deformations, pre-straining, and of a peel-zone model. *J. Adhesion* **84**, 961–995. (doi:10.1080/00218460802576995)
19. Kim KS, Aravas N. 1988 Elastoplastic analysis of the peel test. *Int. J. Solids Struct.* **24**, 417–435. (doi:10.1016/0020-7683(88)90071-6)
20. Hutchinson JW, Suo Z. 1992 Mixed-mode cracking in layered materials. *Adv. Appl. Mech.* **29**, 63–191.
21. Thouless MD, Yang QD. 2008 A parametric study of the peel test. *Int. J. Adhes. Adhes.* **28**, 176–184. (doi:10.1016/j.ijadhadh.2007.06.006)
22. Thouless MD, Jensen HM. 1992 Elastic fracture mechanics of the peel-test geometry. *J. Adhesion* **38**, 185–197. (doi:10.1080/00218469208030454)
23. Tvergaard V. 1990 Effect of fibre debonding in a whisker-reinforced metal. *Mat. Sci. Eng.* **A125**, 203–213. (doi:10.1016/0921-5093(90)90170-8)
24. Hutchinson RG, Hutchinson JW. 2011 Lifetime assessment for thermal barrier coatings: tests for measuring mixed mode delamination toughness. *J. Am. Ceram. Soc.* **94**, S85–S95. (doi:10.1111/j.1551-2916.2011.04499.x)
25. Dorogoy A, Banks-Sills L. 2004 Shear loaded interface crack under the influence of friction: a finite difference solution. *Int. J. Numer. Meth. Engng* **59**, 1749–1780. (doi:10.1002/nme.936)
26. Dorogoy A, Banks-Sills L. 2005 Effect of crack face contact and friction on Brazilian disk specimens—a finite difference solution. *Eng. Fract. Mech.* **72**, 2758–2773. (doi:10.1016/j.engfracmech.2005.05.005)
27. Bascom WD, Bitner JL. 1977 Fracture approach to thick-film adhesion measurements. *J. Mater. Sci.* **12**, 1401–1410. (doi:10.1007/BF00540854)
28. Gent AN, Hamed GR. 1977 Peel mechanics of adhesive joints. *Polym. Eng. Sci.* **17**, 462–466. (doi:10.1002/pen.760170708)
29. Bobyn JD, Wilson GJ, MacGregor DC, Pilliar RM, Weatherly GC. 1982 Effect of pore size on the peel strength of attachment of fibrous tissue to porous-surfaced implants. *J. Biomed. Mater. Res. A* **16**, 571–584. (doi:10.1002/jbm.820160505)
30. Park IS, Yu J. 1998 An X-ray study on the mechanical effects of the peel test in a Cu/Cr/polyimide system. *Acta Mater.* **46**, 2947–2953. (doi:10.1016/S1359-6454(97)00208-5)
31. Sargent JP. 2005 Durability studies for aerospace applications using peel and wedge tests. *Int. J. Adhes. Adhes.* **25**, 247–256. (doi:10.1016/j.ijadhadh.2004.07.005)
32. Kawashita LF, Moore DR, Williams JG. 2005 Comparison of peel tests for metal–polymer laminates for aerospace applications. *J. Adhesion* **81**, 561–586. (doi:10.1080/00218460590954557)
33. Williams JA, Kauzlarich JJ. 2005 The influence of peel angle on the mechanics of peeling flexible adherends with arbitrary load–extension characteristics. *Tribol. Int.* **38**, 951–958. (doi:10.1016/j.triboint.2005.07.024)
34. Randow C, Williams C, Ward T, Dillard D, Dillard J, Wightman JP. 1997 An investigation of the cling of thin polymeric films. *J. Adhesion* **63**, 285–307. (doi:10.1080/00218469708017224)
35. Nase M, Langer B, Grellmann W. 2009 Influence of processing conditions on the peel behavior of polyethylene/polybutene-1 peel systems. *J. Plast. Film Sheet.* **25**, 61–80. (doi:10.1177/8756087909343139)
36. Newby BMZ, Chaudhury MK, Brown HR. 1995 Macroscopic evidence of the effect of interfacial slippage on adhesion. *Science* **269**, 1407–1409. (doi:10.1126/science.269.5229.1407)
37. Newby B, Chaudhury M. 1997 Effect of interfacial slippage on viscoelastic adhesion. *Langmuir* **13**, 1805–1809. (doi:10.1021/la960962c)
38. Newby B, Chaudhury M. 1998 Friction in adhesion. *Langmuir* **14**, 4865–4872. (doi:10.1021/la980290l)
39. Amouroux N, Petit J, Leger L. 2001 Role of interfacial resistance to shear stress on adhesive peel strength. *Langmuir* **17**, 6510–6517. (doi:10.1021/la010146r)
40. Blum F, Gandhi B, Forciniti D, Dharani L. 2005 Effect of surface segmental mobility on adhesion of acrylic soft adhesives. *Macromolecules* **38**, 481–487. (doi:10.1021/ma0485336)
41. Begley MR, Collino RR, Israelachvili JN, McMeeking RM. 2013 Peeling of a tape with large deformations and frictional sliding. *J. Mech. Phys. Solids* **61**, 1265–1279. (doi:10.1016/j.jmps.2012.09.014)
42. Sutton MA, Orteu JJ, Schreier HW. 2009 *Image correlation for shape, motion and deformation measurements*. New York, NY: Springer.
43. Kinloch AJ, Lau CC, Williams JG. 1994 The peeling of flexible laminates. *Int. J. Fracture* **66**, 45–70. (doi:10.1007/BF00012635)
44. Settles GS. 2001 *Schlieren and shadowgraph techniques: visualizing phenomena in transparent media*. Berlin, Germany: Springer.
45. Ogden RW. 1997 *Non-linear elastic deformations*, ch. 4. Mineola, NY: Dover.
46. Suo Z, Hutchinson JW. 1990 Interface crack between two elastic layers. *Int. J. Fracture* **43**, 1–18. (doi:10.1007/BF00018123)
47. Gialamas P, Völker B, Collino RR, Begley MR, McMeeking RM. In press. Peeling of an elastic membrane tape adhered to a substrate by a uniform cohesive traction. *Int. J. Solids Struct.* (doi:10.1016/j.ijsolstr.2014.04.001)
48. Begley MR, Collino RR, McMeeking RM. In preparation. Analysis of peeling of a tape with bending stiffness.
49. Liechti KM, Chai YS. 1991 Biaxial loading experiments for determining interfacial fracture toughness. *J. Appl. Mech.* **58**, 680–687. (doi:10.1115/1.2897248)